

A Numerical Study of Transport and Shot Noise at 2D Hopping

Yusuf A. Kinkhabwala, Viktor A. Sverdlov, and Konstantin K. Likharev
 Department of Physics and Astronomy,
 Stony Brook University, Stony Brook, NY 11794-3800

Alexander N. Korotkov
 Department of Electrical Engineering,
 University of California - Riverside, Riverside, CA 92521

(Dated: January 29, 2020)

We have carried out extensive Monte Carlo simulations of 2D hopping (with negligible Coulomb interaction) in a system with a completely random distribution of localized sites in both space and energy, within a broad range of the applied electric field E and temperature T , both within and beyond the variable-range-hopping region. The calculated properties include dc current, statistics of localized site occupation and hop lengths, and current fluctuation spectrum. Within the calculation accuracy, the model does not exhibit $1/f$ noise, so that the low-frequency noise at low temperatures may be characterized by the Fano factor F . For sufficiently large samples, F scales with conductor length L as $(L_c=L)$, where ≈ 0.76 – 0.08 . The electric field dependence of parameter L_c (interpreted as the average percolation cluster length) is compatible with the law $L_c/E^{0.911}$ following from percolation theory arguments at relatively low E , but attains and approaches the average hop length in very high fields.

PACS numbers: 72.20.Ee, 72.20.Ht, 73.50.Td

I. INTRODUCTION

The theory of hopping transport in disordered conductors,^{1,2,3} without account of electron-electron interaction, is considered a well established (if not completed) field, with the recent research being focused mostly on Coulomb effects. Two factors, however, have motivated us to have a new look at this subject:

1. The literature is surprisingly scarce of quantitative data on major characteristics of hopping, especially in the high-electric-field region ($eE r_{ms} > k_B T$, where r_{ms} is the average hop length) in which dc conductivity becomes a substantial function of E . To the best of our knowledge, the exact location of the crossover to field-independent conductivity (at finite temperature) has never been established. This is not very surprising because virtually the only theoretical technique available for hopping characterization in the high-field region is Monte Carlo modeling, which requires high-performance computing. For example, the work reported below took close to a million processor-hours on modern supercomputers. Such computing resources have become available for the academic solid state physics community only recently.

2. Relatively recently it was recognized that shot noise⁴ is a very important characteristic of electron transport. In particular, the suppression of the current fluctuation density $S_I(f)$ at low frequencies, relative to its Schottky formula value $2ehI$, is a necessary condition for the so-called quasi-continuous ("sub-electron") charge transfer.⁵ Preliminary calculations of shot noise at 1D⁶ and 2D⁷ hopping have shown that such suppression may, indeed, take place. However, the calculations of this ef-

fect for the most important 2D case have been limited to cases of either hopping through very short samples (e.g., across thin $\ln S$)⁹ or in the case of long samples to just one particular value of electric field.⁷ It seemed important to examine whether the law governing this suppression is really as general as it seemed. Such examination, carried out in this work, has become possible only after the development of a new, advanced method of spectral density calculation – see Appendix A.

II. MODEL

We have studied 2D rectangular ($L \times W$) samples with "open" boundary conditions on the interface with well-conducting electrodes⁷ – see inset in Fig. 1. In the present study, we have concentrated on broad samples with width $W \gg L_c$, where L_c is the effective percolation cluster size (see below). The conductor is assumed to be "fully frustrated": the localized sites are randomly distributed over the sample area, and their energies ϵ_j are randomly distributed over a sufficiently broad energy band, so that the 2D density of states is constant at all energies relevant for conduction. Electrons can hop from any site j to any other site k with the rate

$$r_{jk} = r_{jk} \exp \left(-\frac{r_{jk}}{a} \right); \quad (1)$$

where a is the localization radius.¹⁰ Such exponential dependence on the hop length has been assumed in virtually all theoretical studies of hopping. However, in contrast to most other authors, we take Eq. (1) literally even at small distances $r_{jk} \ll a$; this is important only at very

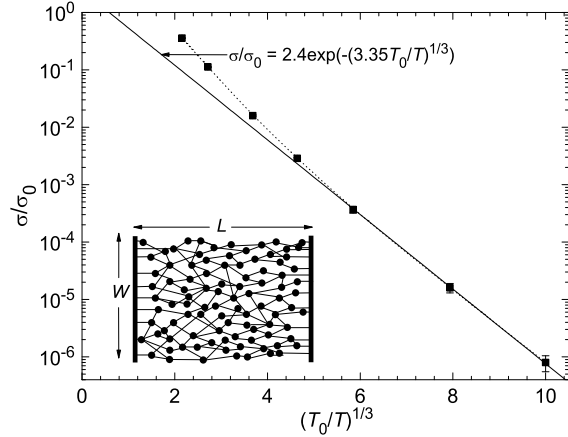


FIG. 1: Linear conductivity σ as a function of temperature T . Points show the results of averaging over 80 samples varying in size ($L \times W$) from $20 \times 10 \text{ \AA}$ to $160 \times 100 \text{ \AA}$, biased by a low electric field $E = E_T$. Points are Monte Carlo results. The dashed line is just a guide for the eye, while the straight line corresponds to the best fit of the data by Eq. (6). Here and below, the error bars are smaller than the point size, unless they are shown explicitly. The error bars correspond to the uncertainty in averaging over an ensemble of independent samples, that is larger than the individual calculational uncertainty for each of the samples. The inset shows the system under analysis (schematically).

high fields and/or temperatures where the average value of r_{jk} becomes comparable to a . Of course our quantitative results for this region are only true for specific confining potentials providing an exponential wave function decay.

Another distinction from some other works in this field is that we assume that the hopping rate amplitude t_{jk} depends continuously on the localized site energy difference $\epsilon_{jk} = \epsilon_j - \epsilon_k + eE r_{jk}$:

$$t_{jk} \sim t_{jk}(\epsilon_{jk}) = g \frac{t_{jk}}{1 + \exp\left(\frac{\epsilon_{jk}}{k_B T}\right)} : \quad (2)$$

This model coincides, for low phonon energies ϵ_{jk} , with that described by Eqs. (4.2.17)–(4.2.19) of Ref. 2, and of course satisfies the Gibbs detailed balance requirement $t_{jk} = t_{kj} \exp(\epsilon_{jk} = k_B T)$. It is also close, but in our view, more natural than the "Metropolis" dependence with a cusp at $\epsilon_{jk} = 0$.

The interaction of hopping electrons is assumed negligible, with the exception of the implicit Pauli-principle interaction, i.e. no hopping to already occupied sites.

Scales of all variables within our model are natural combinations of the constants a and σ_0 (plus temperature T , applied electric field E , and fundamental constants). In particular, there are three possible energy scales: $k_B T$, $eE a$, and $\sigma_0 a^2$. This means that there are two char-

acteristic values of electric field:

$$E_T = \frac{k_B T}{ea}; E_0 = \frac{1}{e a^3} : \quad (3)$$

We will be mostly interested in the case of low temperatures, $T < T_0$, where

$$T_0 = \frac{1}{k_B a^2} \quad (4)$$

is the field-independent scale of temperature, so that $E_T < E_0$.

Note that the only role of the dimensionless parameter g introduced by Eq. (2) is to participate in the scale of hopping conductivity

$$\sigma_0 \sim \frac{e^2}{\tau} : \quad (5)$$

In order to keep coherent quantum effects leading to weak localization and metal-to-insulator transition negligibly small, and hence the formulated hopping model possible, g should be much less than unity.

The dynamic Monte Carlo calculations were carried out using the algorithm suggested by Bakhvalov et al.,¹¹ which has become the de facto standard for single-electron tunneling simulations.¹² All calculated variables were averaged over the sample, and in most cases, over several (many) samples with independent random distributions of localized sites in space and energy, but with the same dimensionless parameters $L=a, W=a, T=T_0$, and $E=E_0$. For the purposes of this work, the noise, i.e. current spectral density, calculation technique has been modified (see Appendix A).

III. DC CURRENT AND HOPPING STATISTICS

In order to understand the relation between our model and the prior results in this field, we have started from the calculation of dc current $\langle I \rangle$ as a function of T and E . If the electric field is small, $E = E_T$, then the current is proportional to E , and the transport is completely characterized by the linear conductivity $\langle I \rangle = W E$. Fig. 1 shows the calculated conductivity as a function of temperature T ; in the whole region $T < T_0$ this dependence follows the 2D Mott law^{1,2,3}

$$\sigma = A T_0 \exp\left(-B T \frac{T_0}{T}\right)^{\#} ; \quad (6)$$

within the accuracy of our numerical experiments. For the constants participating in this expression, fitting gives the following values

$$A_T = 2.4 \pm 0.1; B_T = 3.35 \pm 0.12 : \quad (7)$$

This result for B_T should be compared with the following values reported in the literature: $2.2^{1,3}$, 3.45^2 and

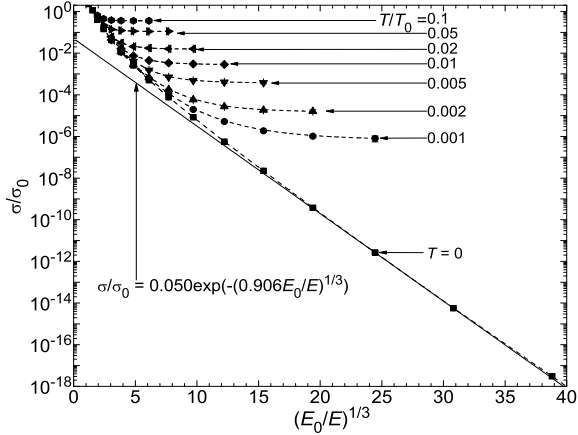


FIG. 2: Nonlinear conductivity σ/σ_0 as a function of electric field E for several values of temperature T . Each point represents data averaged over 80 samples of the same size (ranging from $20 \times 14a^2$ to $1000 \times 700a^2$, depending on T and E). Points are Monte Carlo results. Dashed lines are only guides for the eye, while the straight line shows Eq. (8) with the best-fit values of A_E and B_E .

325.¹⁴ The differences are possibly due to that of the slightly different models for the function χ_k (χ_k) (see Sec. II above).

At higher electric fields ($E > E_T$), dc current starts to grow faster than the Ohm law, so that if we still keep the above definition of conductivity, it starts to grow with E (Fig. 2). At $T \neq 0$, the results are well described by the "high-field" equation⁷

$$\sigma = A_E \exp\left(-B_E \frac{E_0}{E}\right)^{1/3}; \quad (8)$$

with

$$A_E = 0.050 \quad 0.005; B_E = 0.906 \quad 0.015; \quad (9)$$

The latter value is close to the result ($B_E = 1.27$) given in Ref. 7, while the new value for the pre-exponent A_E is significantly different from the previous estimate (0.05) that had been made from calculations in a narrower range of electric fields. (Note that small errors in B_E may lead to large changes of the best-fit for A_E .)

Finally, Fig. 2 shows that when the electric field becomes comparable with the value E_0 defined by the second of Eqs. (3), dc current and hence, conductivity, start to grow even faster than that given by Eq. (8).

In order to understand the physics of hopping in these three field regions better, it is very useful to have a look at the statistics of localized site occupation and hopping length. We have found that for all studied values of E and T , the probability of site occupation closely follows the Fermi distribution with the local Fermi level

$$f(\epsilon) = \frac{1}{1 + \exp(\epsilon - E_{\text{eff}}/k_B T)} \quad (10)$$

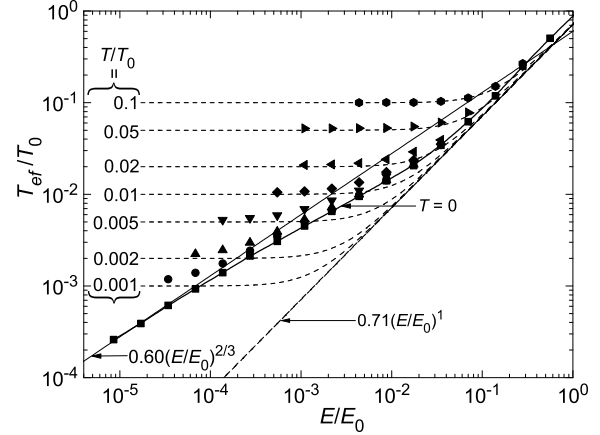


FIG. 3: The effective temperature T_{eff} of current carriers as a function of electric field E for several values of temperature T . Closed points: Monte Carlo (MC) simulation results; dashed lines: master equation (ME) results. The solid curve marked $T = 0$ is only a guide for the eye.

(where ϵ_L is the Fermi level of the source electrode) and some effective temperature T_{eff} . Points in Fig. 3 show T_{eff} as a function of electric field E for several values of physical temperature T . Dashed lines show the result of the best fitting of the naive single-particle master equation

$$\frac{\partial f(\epsilon; t)}{\partial t} = \sum_r \sum_r' \left[\frac{1}{a} \exp\left(\frac{\epsilon_r - \epsilon_{r'}}{a}\right) f(\epsilon_r) [1 - f(\epsilon_{r'})] + \frac{1}{a} \exp\left(\frac{\epsilon_{r'} - \epsilon_r}{a}\right) f(\epsilon_{r'}) [1 - f(\epsilon_r)] \right] \quad (11)$$

by a stationary Fermi distribution. Equation (11) would follow from our model if percolation effects were not substantial. At real hopping, we can expect the results following from Eq. (11) to be valid only in certain limits.¹⁵ For example, in the low field limit, $E \ll 0$, both methods give $T_{\text{eff}} = T$. At higher electric fields the effective temperature grows with the applied field, which "overheats" the electrons. At very high fields ($E/E_0 > 0.3$) both methods agree again and give

$$k_B T_{\text{eff}} = C e E a; \quad C = 0.71 \quad 0.02; \quad (12)$$

(A similar result, but with $C = 1.34$, for our definition of a , was obtained by Marianer and Shklovskii¹⁶ for a rather different model with an exponential energy dependence of the density of states.) However, at intermediate fields, $E_T < E < E_0$ (this regime is frequently called "high-field variable-range-hopping"), the master equation still gives the same result (12) and hence fails to appreciate that in fact T_{eff} is proportional to $E^{2/3}$. In order to explain this result, let us discuss the statistics of hopping lengths (Figs. 4 and 5).

The two- and one-dimensional histograms in Fig. 4 show the probability density P of a hop between two sites separated by the vector \mathbf{r} , and also the density P_d weighed by the factor $\sum_{j;k} N_{jk} N_{kj}$, where each N is the total number of hops (during a certain time interval) in the indicated direction. The latter weighing emphasizes the site pairs $(j;k)$ contributing substantially to the net hopping transport, in comparison with "blinking" site pairs, which exchange an electron many times before allowing it to advance along the field. It is clear that at relatively high temperatures or low fields ($E < E_T$) the non-weighted distribution should be symmetric (Fig. 4a). Fig. 4d shows that in this case the one-dimensional probability density is well approximated by the Rayleigh distribution, $P(r) / r \exp(-r/a)$. However, the weighed hop distribution is strongly asymmetric even in the limit $E \rightarrow 0$ (Fig. 4b). This asymmetry is even more evident at low temperatures or high fields ($E > E_T$); in this case the distribution has a sharp boundary (Fig. 4c). Fig. 4d shows those cases where the 1D histograms deviate substantially from the distribution predicted by the master equation (see Eq. (19)).

Figure 5 shows the r.m.s. non-weighted (r_{rms}) and direction-weighted (r_{rmsd}) hop lengths, defined, respectively, as

$$r_{rms}^2 = \frac{\sum_{j;k} P_{jk} r_{jk}^2 N_{jk} + \sum_{k;j} P_{kj} r_{kj}^2 N_{kj}}{\sum_{j;k} (N_{jk} + N_{kj})} \quad (13)$$

and

$$r_{rmsd}^2 = \frac{\sum_{j;k} P_{jk} r_{jk}^2 N_{jk} + \sum_{k;j} P_{kj} r_{kj}^2 N_{kj}}{\sum_{j;k} N_{jk} + \sum_{k;j} N_{kj}} \quad (14)$$

(that are of course just the averages of the histograms shown in Fig. 4), as functions of applied electric field for several values of temperature. At $T \rightarrow 0$, hopping is strictly one-directional (i.e., if $N_{jk} \neq 0$, then $N_{kj} = 0$), so that r_{rms} and r_{rmsd} should be equal. In fact, simulation shows that in this limit both lengths coincide, at lower fields following the scaling⁷

$$r_{rms} = r_{rmsd} = D a \frac{E_0}{E}^{1/3}; \quad E_T < E < E_0; \quad (15)$$

with $D = 0.72 \pm 0.01$. (We are not aware of any prior results with which this value could be compared.)

This scaling of r in the variable-range-hopping region is essentially the reason for the scaling of T_{ef} mentioned above; in fact, the hopping electron gas "overheating" may be estimated by equating $k_B T_{ef}$ to the energy gain $eE r_{rms}$, possibly multiplied by a constant of the order of one. For the effective temperature, this estimate gives

$$k_B T_{ef} = \text{const } eE r_{rms} = G e a E_0^{1/3} E^{2/3} = G \frac{(E = E_0)^{2/3}}{a^2}; \quad (16)$$

in accordance with the result shown in Fig. 3. For constant G our Monte Carlo simulations give the value 0.60 ± 0.02 ; we are not aware of any previous results this number could be compared with.

At higher fields ($E > 0.1E_0$) the hop lengths start to decrease slower, approaching a few localization lengths a (Fig. 5a). In this ("ultra-high-field") region, the energy range $eE a$ for tunneling at distances of a few a is so high that there are always some accessible empty sites within this range, so that long hops, so dominant at variable range hopping, do not contribute much into conduction.

At finite temperatures, the most curious result is a non-monotonic dependence of the r.m.s. hopping length on the applied field - see Fig. 5a. At $E \rightarrow 0$, r_{rms} has to be field-independent, and there is no scale for it besides a . (As evident as it may seem, this fact is sometimes missed in popular descriptions of hopping.) In order to make a crude estimate of r_{rms} in this limit, one can use the master equation Eq. (11). In this approach, at thermal equilibrium (i.e. at independent of r), the hop length probability density $P(r)$ can be found as

$$P(r) = \frac{\sum_{j;k} \sum_{l;m} P_{jk} P_{lm} r_{jk} r_{lm} \exp(-r/a)}{\sum_{j;k} (N_{jk} + N_{kj})} \quad (17)$$

in a good agreement with the results shown in Fig. 4d for this case. From Eq. (17), we get

$$r_{rms}^2 = \frac{\int_0^\infty P(r) r^2 dr}{\int_0^\infty P(r) dr} = \frac{\int_0^\infty P(r) r^2 dr}{\int_0^\infty P(r) dr} = \frac{P}{6a} = 2.45a; \quad (18)$$

in a good agreement with numerical data shown in Fig. 5.

A similar calculation for r_{rmsd} may be obtained by expanding the tunneling rate $(\sum_{j;k} P_{jk} + eE r)$ in small electric field as $(\sum_{j;k} P_{jk} + eE r)$. The result is

$$P_d(r) = \frac{\sum_{j;k} \sum_{l;m} P_{jk} P_{lm} r_{jk} r_{lm} \exp(-r/a)}{\sum_{j;k} (N_{jk} + N_{kj})} \quad (19)$$

The Monte Carlo data (Fig. 5), however, differ from this result, showing that at $E \rightarrow 0$, r_{rmsd} obeys the Mott law^{1,2,3}

$$r_{rmsd} = H a \frac{T_0}{T}^{1/3} + I a; \quad T > T_0; \quad (20)$$

with the best-fit values $H = 0.52$, 0.05 and $I = 2.0$, 0.1 .¹⁸ In contrast, the function $r_{rms}(T)$ is rather far from Eq. (20), because the Mott law refers to long hops responsible for transport (with the average approximately corresponding to r_{rms}), while r_{rms} reflects the statistics of all hops.

To summarize, our results for average conductivity and hop statistics confirm that our model gives a reasonable description of the well-known picture of hopping, including the usual variable range hopping at low fields ($E = E_T$) and "high-field variable range hopping" at $E_T < E < E_0$. Moreover, the model also describes the "ultra-high field" region ($E > E_0$) where the variable range hopping picture is no longer valid, since from most localized sites an electron can hop, with comparable probability, to several close sites. In the last region, there is no single percolation cluster isolated in the sample; rather, electrons follow a large number of interwoven trajectories.

IV. SHOT NOISE

The achieved understanding of hopping characteristics within our model has helped us to interpret the results of current noise simulation. This simulation was limited to the case of low temperatures ($E_T < E$). (In the opposite limit, noise is described by the fluctuation-dissipation theorem; its low-frequency intensity can be found from (T) and does not require a special calculation.)

The largest practical problem with the noise evaluation is that the calculation of spectral density $S_I(f)$ of current fluctuations with acceptable accuracy typically requires much larger statistical ensemble of random samples than that of the average current. This is why, even with an advanced algorithm for spectral density calculation (see Appendix A), noise calculation has required very substantial supercomputer resources.

Figure 6 shows a typical dependence of the current noise spectral density S_I , normalized to the Schottky value $2ehI$, on the observation frequency $\omega = 2\pi f$. One can see a crossover from a low-frequency plateau to another plateau at high frequencies. As the sample length grows, the crossover becomes extended, i.e. features a broad intermediate range $\omega_1 < \omega < \omega_h$, just like in 1D systems with next-site hopping.⁶ The position of the high-frequency end ω_h of this region can be estimated in the following way. In all single-electron systems, the high-frequency plateau is reached at frequency ω_h close to the rate of the fastest electron hops affecting the total current.^{6,7,19,20} (For example, in systems described by the orthodox theory of single-electron tunneling, $\omega_h \approx \omega_{max} = e^2 R^{-1} = RC^{-1}$, where R and C are, respectively, resistance and capacitance of a single junction.^{19,20}) In our current case, this means that $\omega_h \approx (\nu_{jk})_{max} \approx (g \sim 1) [\nu_{jk} \exp(\nu_{jk} a)]_{max}$. For this estimate, ν_{jk} can be taken as $k_B T_{ef}$ from Fig. 3, while according to the histograms shown in Fig. 4 (d), the length

of shortest hops still giving a noticeable contribution to the current, can be estimated as $r_{rms} = 2$. For the case shown in Fig. 6 ($E = E_0 = 8.75 \cdot 10^3$), these estimates yield $\nu_{jk} \approx k_B T_{ef} \approx 2 \cdot 10^2$, $(r_{jk})_{min} \approx a \approx 2.5$, giving finally $\omega_h \approx 1.5 \cdot 10^3$, in a very reasonable agreement with numerical results shown in Fig. 6. (Note that this simple estimate, giving a length-independent value for ω_h , is only valid for relatively long and broad samples.)

At $\omega \approx \omega_h$, a crossover to $1/f$ noise might be expected, because the discussion of this effect in some earlier publications^{21,22} was apparently independent of the Coulomb interaction between hopping electrons. However, within the accuracy of our simulations, we could not find any $1/f$ -type noise for any parameters we have explored. We have not found this fact very surprising, because all the discussions of the $1/f$ noise we are aware of require the presence of thermal fluctuations. In our case ($T = 0$) these fluctuations are absent.

Since the low-frequency spectral density is flat, at $T = 0$ it may be considered as shot noise²³ and characterized by the Fano factor⁴

$$F = \frac{S_I(f \ll \omega_h)}{2ehI} \quad (21)$$

Similarly, in order to characterize the flat high-frequency spectral density, we may use the parameter

$$F_1 = \frac{S_I(f \gg \omega_h)}{2ehI} \quad (22)$$

Figure 7 (a) shows the average Fano factors F and F_1 as a function of L for several values of the applied electric field, while Fig. 7 (b) shows that the same data can be collapsed on universal curves by the introduction of certain length scales: L_c for F and L_h for F_1 .

For the high frequency case,

$$F_1 = \frac{L_h}{L} \quad ; \quad L \gg L_h \quad (23)$$

where, within the accuracy of our calculations, $L_h = 1$. Such dependence could be expected, because the high-frequency noise at hopping can be interpreted as a result of "capacitive division" of the discrete increments of externally-measured charge jumps resulting from single-electron hops through the system.²⁴ When applied to uniform (ordered) systems, these arguments always give the result $F_1 = 1/N_h$ with $N_h = L/d$ being the number of electron hops (d the hopping length along the current flow) necessary to pass an electron through the system, regardless of hop rates.^{4,5,6} For $T = 0$ in the case of disordered conductors, L_h in Eq. (23) may then be interpreted as essentially the average hop length along current flow. This interpretation turns out to be true: Figure 8 shows that the parameter L_h obtained from Eq. (23) scales with the electric field in a similar manner as r_{rms} , especially at low fields, where it follows the variable range hopping dependence of Eq. (15).

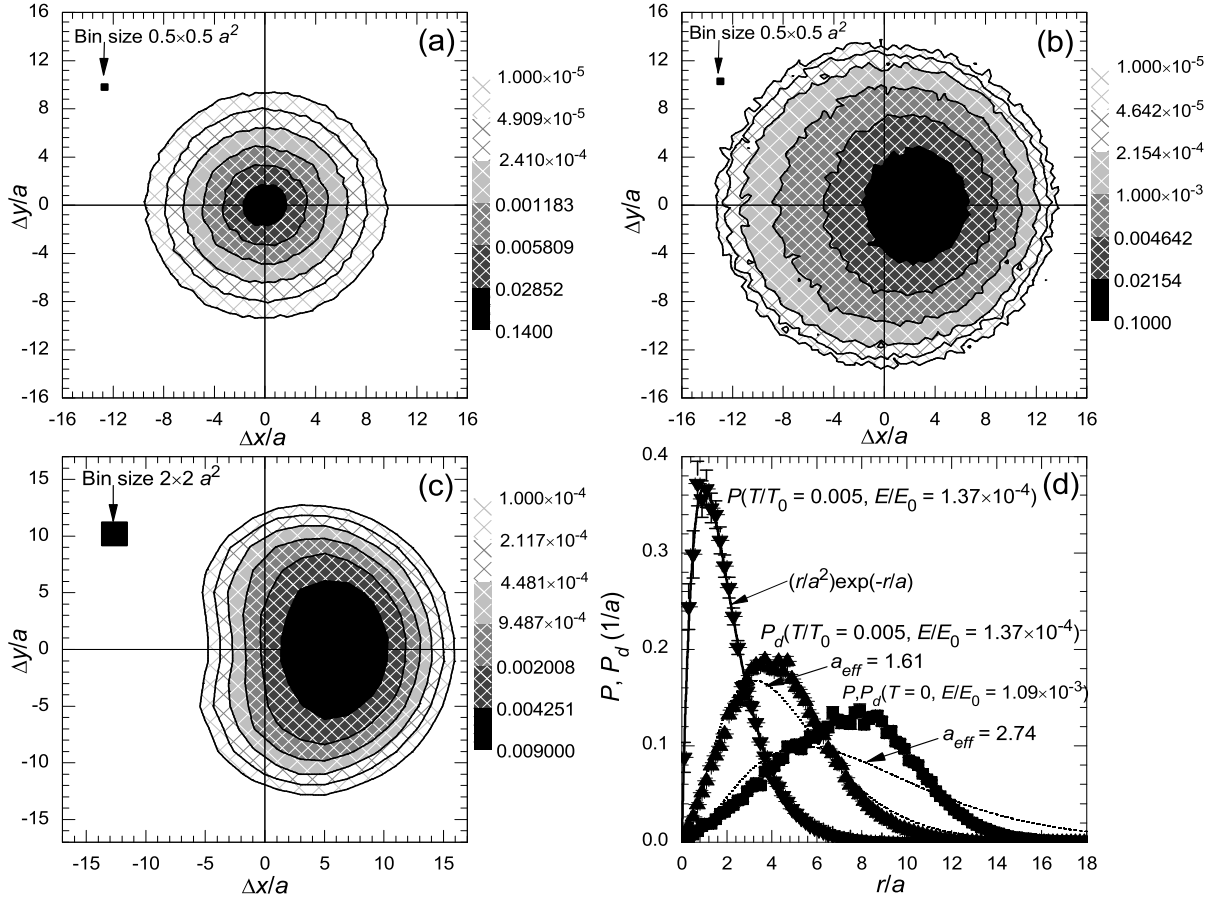


FIG. 4: (a)–(c) Two-dimensional and (d) one-dimensional histograms of hop lengths for two typical cases: (a) and (b): $T=T_0 = 5 \cdot 10^3$, $E=E_0 = 1.37 \cdot 10^4$ ($E > E_T$) and (c): $T=0$, $E=E_0 = 1.09 \cdot 10^3$ ($E_T > E$). The shade-coding in panels (a) and (c) is proportional to the probability P of hops with given $r = (x, y)$, while that in panel (b), to the probability P_d weighed by factor $\sum_{j,k} N_{k,j} N_{j,k}$ – see the text. (Since at $T=0$ there are no backward hops, for the case shown in panel (c), P and P_d coincide.) Panel (d) shows P and P_d , averaged over all angles of vector r , for both the high-eld and low-eld case. Dashed lines show the distribution (19) given by master equation, for best-fit values of a_{eff} .

The results for F_m may be also reasonably well fit with a universal dependence on $L=L_c$. For long samples, the dependence approaches⁷

$$hFi = \frac{L_c}{L}; \quad L \gg L_c: \quad (24)$$

Here α is a numerical exponent; in the current study we could establish that

$$\alpha = 0.76 \pm 0.08: \quad (25)$$

Eq. (24) and the value for α is compatible with our previous results⁷ $\alpha = 0.85 \pm 0.07$ (for the same model as now, for one particular value of E) and $\alpha = 0.85 \pm 0.02$ (for nearest neighbor hopping on uniform slanted lattices). In

the thin limit ($L \ll L_c$) the average Fano factor is weakly dependent on length and approaches $hFi \approx 0.7$, consistent with the prior results for hopping on 1-site chains⁸ ($hFi = 0.75$) and 2-site chains⁹ ($hFi = 0.707$).

Figure 8 shows the fitting parameter L_c as a function of electric field E . In the variable range hopping region, it may be fitted with the following law,

$$L_c = J a \frac{E_0}{E}; \quad J = 0.04 \pm 0.01; \quad \alpha = 0.98 \pm 0.08: \quad (26)$$

This law may be interpreted in the following way. The parameter L_c is essentially the average percolation cluster length (up to a constant of the order of 1).⁷ The theory of directed percolation^{25,26,27} gives the following

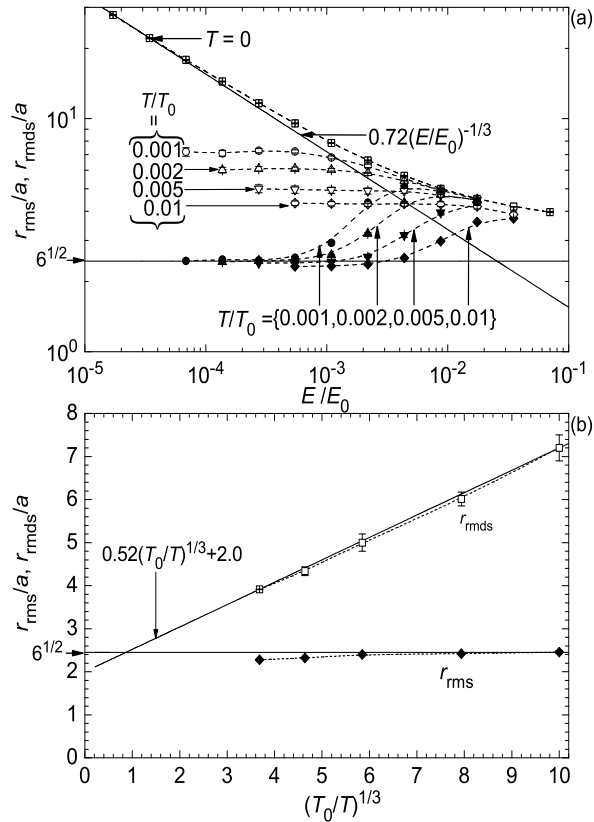


FIG. 5: R m s. hop length r_{rms} (solid points) and the weighed average hop length r_{rms}^w (open points) as functions: (a) of applied electric eld E for several temperatures T , and (b) of temperature at $E = 0$. Tilted straight lines in panels (a) and (b) show the best ts by Eqs. (15) and (20), respectively, while the horizontal thin lines show the values following from the master equation. Curves are only guides for the eye.

scaling:

$$L_c / \langle x_i \rangle = \frac{x_c}{\langle x_j \rangle}^k : \quad (27)$$

Here $\langle x_i \rangle$ is the r m s. hop length along the eld direction, x_c is its critical value, and the critical index k should be close to 1.73.²⁷ Due to the exponential nature of the hopping, $\langle x_i \rangle \propto a$, while $\langle x_j \rangle$ should follow eld scaling similar to that given by Eq. (15). (Square points in Fig. 8 show that this is true for our simulation results as well.) Thus for sufficiently large $\langle x_i \rangle$ we arrive at Eq. (26) with $k = \frac{1}{3} + \frac{1}{k} \approx 0.911$. This value is compatible with our numerical result, thus confirming the interpretation of L_c as the average percolation cluster length.

Note that in the variable range hopping regime L_c has a different eld dependence, and is much larger than the average hop length. However, as the applied electric eld approaches E_0 , both lengths become comparable with

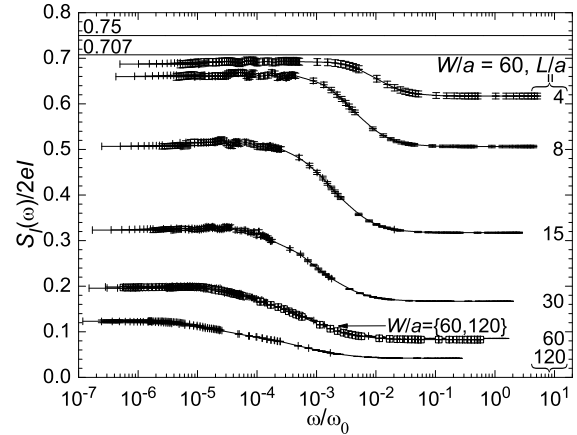


FIG. 6: Spectral density S_I of current uctuations normalized to the Schottky noise $2ehI_0$ as a function of observation frequency ω , measured in units of $\omega_0 = g_0 a^2$, for several values of sample length L for $T = 0$ and $E = E_0 = 8.75 \cdot 10^3$. Small points show results for $W = a = 60$, while open squares are for $W = a = 120$ (at $L = a = 60$). Horizontal lines correspond to the Fano factor for hopping through short samples with one and two localized sites.^{8,9} Curves are only guides for the eye.

each other and with the localization radius a .

V. DISCUSSION

Our simulations of shot noise at 2D hopping have confirmed our earlier hypothesis that in the absence of substantial Coulomb interaction, in sufficiently large samples ($L; W \gg L_c$) the Fano factor F scales approximately proportionally to $1/L$ – see Eq. (24). Other confirmations of this hypothesis have come from recent experiments with lateral transport in SiGe quantum wells²⁸ and GaAs MESFET channels.²⁹ Unfortunately, these experiments are not precise enough to distinguish the small difference between the exponent in Eq. (24) from unity.

The hypothesis that F is in fact equal to 1 for sufficiently long samples seems appealing, because it would mean the simple addition of mutually-independent noise voltages generated by sample sections connected in series. On the contrary, a deviation of F from unity would mean that dynamic correlations of electron motion in percolation clusters persist even at $L \gg L_c$. We can present, as an example, at least one exactly solvable model (the "asymmetric single exclusion process", or ASEP³⁰) in which the dynamic correlations may change from 1 to 0.5. (It is instructive to notice that in the ASEP model the dynamic correlations do not affect average transport characteristics, and may be ignored, in particular, in calculations of dc current.) One more remark we can offer is

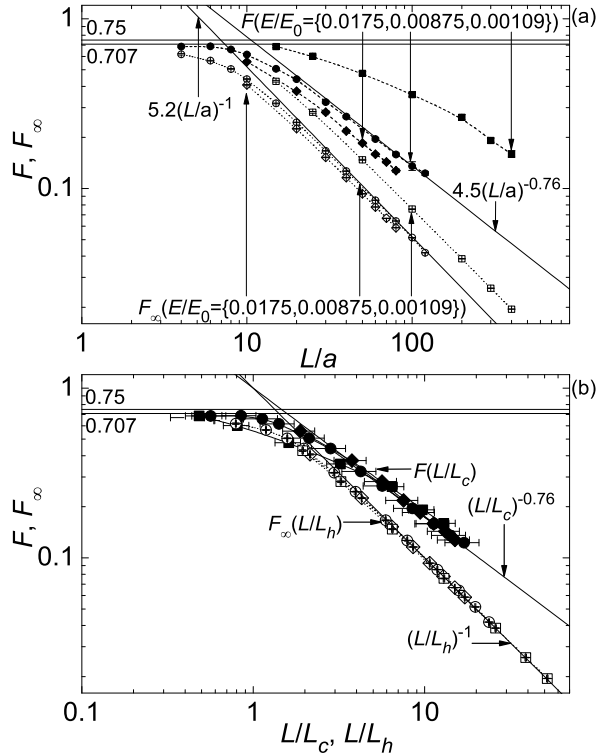


FIG. 7: A average Fano factor F and its high-frequency counterpart F_1 as functions of sample length L normalized to: (a) the localization length a , and (b) the scaling lengths L_c (for F) and L_h (for F_1) (see Fig. 8 below), for several values of applied field at $T = 0$ and $W = L_c$. Horizontal lines correspond to the average Fano factor for hopping via one and two localized sites.^{9,9} Straight lines are the best fits to the data, while dashed curves are only guides for the eye.

that the value of F following from our calculations (0.76) does not violate any scaling laws. On the other hand, at this stage we cannot exclude the possibility that F will tend closer to one (say, logarithmically) in extremely long samples. Moreover, our preliminary results for finite Coulomb interaction show that in this case F does in fact approach one in sufficiently large conductors.

From the point of view of possible applications in single-electron devices,³¹ the fact that F may be suppressed to values much less than unity, may seem encouraging, since it enables the use of circuit components with quasi-continuous charge transport for the compensation of random background charge in single-electron islands. However, in order to achieve the really quasi-continuous transfer (say, $F < 0.1$), the sample length L has to be an order of magnitude longer than the percolation cluster length scale L_c . On the other hand, L_c itself, especially in the most interesting case of low applied field, is much longer than the localization length a (Fig. 8), which is of

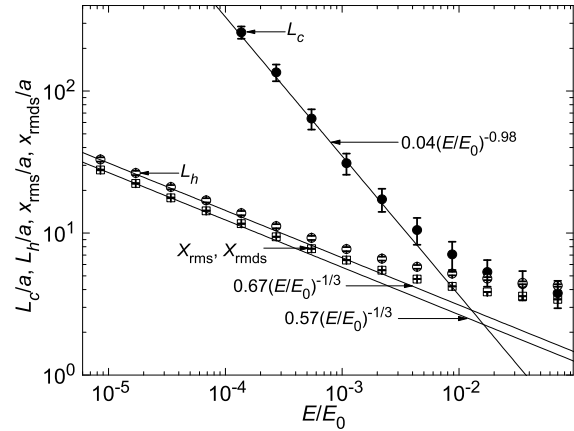


FIG. 8: The values of L_h and L_c giving the best fitting of shot noise results by Eqs. (23) and (24) as functions of applied electric field (open and solid circles, respectively). Open squares show the simple and direction-weighted average hop length along the applied field direction, defined similarly to Eqs. (13) and (14). Straight lines are the best fits to the data.

the order of 1 nm in most prospective materials. Hence, it may be hard to implement sub-electron transport in components substantially smaller than 100 nm. This size is probably too large for future room-temperature single-electron circuits,³¹ because of large stray capacitance that effectively adds up to the capacitance of the island to be serviced.

Acknowledgments

Fruitful discussions with B. Shklovskii and D. Tsiganov are gratefully acknowledged. The work was supported in part by the Engineering Physics Program of the Office of Basic Energy Sciences at the U.S. Department of Energy. We also acknowledge the use of the following supercomputer resources: SBU's cluster Njall (purchase and installation funded by DOD's DURIP program via AFOSR), Oak Ridge National Laboratory's IBM SP computer Egle (funded by the Department of Energy's Office of Science and Energy Efficiency program), and also IBM SP system Tempest at Maui High Performance Computing Center and IBM SP system Habu at NAVO Shared Resource Center (computer time granted by DOD's High Performance Computing Modernization Program).

APPENDIX A: FAST ALGORITHM FOR SPECTRAL DENSITY CALCULATION

In this Appendix we describe the numerical algorithm used for the Monte Carlo calculation of the spectral den-

sity $S_I(\omega)$ of the hopping current $I(t)$. (This algorithm has been also used, without explanation, in our earlier papers.^{6,7,32}) Besides calculation of noise in hopping, the method is applicable to the spectral density of tunneling current in multi-junction single-electron devices²⁴ because of the problem similarity.

The first spectral calculations of the electron transport in single-electron devices using the Monte Carlo technique have been performed in Refs. 11 and 33; in these papers the spectral density has been calculated as a Fourier transform of the correlation function. However, this method is rather slow in the case when the current $I(t)$ is a sequence of δ -functions, corresponding to tunneling events:

$$I(t) = \sum_n q_n \delta(t - t_n); \quad (\text{A } 1)$$

where t_n is a (random) time of the n -th tunneling event and q_n is the corresponding charge transfer. (The sequence q_n is also random and reflects the path in the space of charge configurations.)

A significantly faster "standard" algorithm²⁰ (embedded, for example, into the simulation package MOSES³⁴) is based on the definition of the spectral density $S_I(\omega)$ of the current $I(t)$ via the square of the Fourier transform $|\tilde{I}(\omega)|^2$. More specifically, for the rectangular time window (natural in simulations) there is a relation

$$\frac{2}{T} \int_{t_0}^{t_0+T} I(t) \exp(i\omega t) dt = \sum_n S_I(\omega + \frac{2\pi n}{T}) \frac{1 - \cos(\omega T)}{T^2} \quad (\text{A } 2)$$

(here $\langle \dots \rangle$ denotes ensemble averaging and i in this Appendix is the imaginary unit), whose right hand side tends to $S_I(\omega)$ in the limit $T \rightarrow \infty$. Therefore,

$$S_I(\omega) \approx \frac{2}{T} \sum_n q_n \exp(i\omega t_n) \quad (\text{A } 3)$$

is a good approximation for the true spectral density $S_I(\omega)$ even for a finite, but large enough time interval T . (Summation in Eq. (A 3) is over the tunneling events within the interval $t_0 < t_n < t_0 + T$). In the standard method^{20,34} the ensemble averaging in Eq. (A 3) is replaced by averaging over K sequential time segments (each of duration T) of the Monte Carlo realization, so that t_0 becomes jT , where $j = 1, 2, \dots, K$. It is natural to calculate simultaneously the spectral density for a set of frequency points (the set of harmonics of a certain low frequency is most convenient), and it is useful to choose $K=2$ equal to integer multiples of T^{-1} to avoid "poisoning" of the right hand side of Eq. (A 2) by the δ -function contribution from $S_I(0)$ due to dc current \bar{I} . (Other ways of subtracting the effect of \bar{I} are also possible.)

A major disadvantage of this standard method is that the relative accuracy of the spectral density calculation

cannot be better than approximately $K^{-1/2}$, because the right hand side of Eq. (A 3) before averaging over K segments has the same fluctuation comparable to the mean value. It is easy to increase K (without increasing the total simulation time) by decreasing T ; however, besides increasing the smoothing of $S_I(\omega)$ [which is $\propto T^{-1}$ (see Eq. (A 2))], this may lead to incorrect results when T becomes comparable or less than the longest correlation time of the simulated process, and therefore the T -segments are no longer statistically independent. Since the correlation time is not known in advance (it may be estimated as the lowest frequency at which the spectral density levels off), the choice of T is not a trivial task and requires some intuition that complicates the use of the standard method.

Here we describe the advanced algorithm of spectral density calculation which eliminates this problem and also makes calculation significantly faster (for the same accuracy of the result). The method is somewhat similar to the "reduced" method for dc current calculation²⁰ and basically treats the randomness of tunneling times t_n analytically, while the path in the charge configuration space is still simulated¹¹ by the Monte Carlo technique.

Let us consider a T -long realization of the process assuming for simplicity $t_0 = 0$, so that $t_n = \sum_{k=1}^n \tau_k$ where τ_k is the time between the adjacent tunneling events, i.e. time spent in a particular charge state. In the case when the system parameters (external voltage, etc.) do not change with time, the random time τ_k has the Poisson distribution with the average value $\langle \tau_k \rangle = 1/h_k$, where h_k is the sum of all tunneling rates for the corresponding charge state. The quantity $s = \sum_n q_n \exp(i\omega t_n)$, which is related to the spectral density via Eq. (A 3), may be easily expressed as

$$s = \sum_{n,m} q_n q_m \exp(i\omega \sum_{k=1}^n \tau_k) \sum_{k=1}^n \sum_{k=1}^m \exp(i\omega \tau_k) = \sum_n q_n^2 + 2 \operatorname{Re} \sum_{n>m} q_n q_m \exp(i\omega \sum_{k=m+1}^n \tau_k) \quad (\text{A } 4)$$

For the ensemble averaging of s let us first average Eq. (A 4) over random τ_k , leaving averaging over paths in charge space for later. Using the mutual independence of τ_k fluctuations, we can average each exponent independently:

$$\langle \exp(i\omega \tau_k) \rangle = \int_0^\infty \frac{e^{-h_k \tau} e^{i\omega \tau}}{h_k} d\tau = \frac{1}{1 - i\omega / h_k}; \quad (\text{A } 5)$$

thus obtaining the expression

$$\langle |s|^2 \rangle = \sum_n q_n^2 + 2 \operatorname{Re} \sum_{n>m} q_n q_m \sum_{k=m+1}^n \frac{1}{1 - i\omega / h_k} \quad (\text{A } 6)$$

This expression can be calculated iteratively introduc-

ing complex variables

$$A_p = \sum_{n=1}^{X^p} c_n^2 + 2 \sum_{n>m}^{X^p} c_n c_m \sum_{k=m+1}^{Y^n} \frac{1}{1 - i! h_k i}; \quad (A 7)$$

$$B_p = \sum_{m=1}^{X^p} c_m \sum_{k=m+1}^{Y^p} \frac{1}{1 - i! h_k i}; \quad (A 8)$$

that satisfy recurrent equations

$$A_{p+1} = A_p + c_{p+1}^2 + 2c_{p+1} B_p \frac{1}{1 - i! h_{p+1} i}; \quad (A 9)$$

$$B_{p+1} = c_{p+1} + B_p \frac{1}{1 - i! h_{p+1} i}; \quad (A 10)$$

with initial condition $A_0 = B_0 = 0$, while $h_{p+1} = \text{Re} A_p$ at the end of realization.

It is important to notice that $\text{Re} A_p$ accumulates with the length of realization (in contrast to s before averaging, which is a strongly fluctuating variable), so that $(2 = h_{p+1} i) \text{Re} A_p$ (where $h_{p+1} i = \sum_k c_k h_k i$) tends to some limit at $p \rightarrow \infty$. This is the reason why, in contrast to the standard method, the numerical averaging over many T -segments is not necessary now, and the ensemble averaging of the segments over different realizations can be replaced by the natural "time" averaging over the length of a realization. This eliminates the problem of choosing T , discussed above, and now T can be treated as a running variable $T_p = h_{p+1} i$ during the whole simulation run. Similarly, s can also be treated as a running variable s_p . (Strictly speaking, averaging over k in the segments with a fixed time T and/or a fixed charge path is different; however, the difference vanishes at large T .)

Thus, the basic algorithm is the following. The Monte Carlo technique is used to simulate one long realization of the random path in the configuration (charge) space, while the time is treated deterministically as $\sum_k h_k i$; the variables A_p and B_p are updated after each tunneling event using Eqs. (A 9)–(A 10), and the current spectral density $S_I(\omega)$ is calculated as

$$S_I(\omega) = \frac{2}{h_{p+1} i} \text{Re} A_p; \quad (A 11)$$

Even though breaking the simulation into segments is not needed in the new method, the calculation and comparison of partial results for $S_I(\omega)$ on some time segments is useful for run-time estimates of the calculation accuracy.

Actually, this basic algorithm still requires several improvements to become faster than the standard method, especially at low frequencies. First, the accuracy can be significantly improved by explicitly calculating the spectral density for the function $I(t) - \bar{I}$ instead of $I(t)$. (The average current \bar{I} can be calculated as $\sum_k c_k h_k i$, which is the same as in the reduced method^{20,34}.) For this purpose the definition of quantity s should be modified to $s_p = \frac{1}{P} \sum_n c_n \exp(i! t_n) - \bar{I} \exp(i! t_p) = \frac{1}{P} \sum_n c_n \exp(i! t_n) - \bar{I} (1 - \exp(-i! t_p)) = i! t_p$. From

this point, the derivations are similar to those discussed above, though are now significantly lengthier. The final result is that the only change in the algorithm is a different set of recurrent equations replacing Eqs. (A 9)–(A 10):

$$A_{p+1} = A_p + c_{p+1}^2 - 2\bar{I} h_{p+1} i \frac{c_{p+1} \bar{I} h_{p+1} i}{1 + (h_{p+1} i)^2} + 2 \frac{c_{p+1} \bar{I} h_{p+1} i}{1 - i! h_{p+1} i} B_p; \quad (A 12)$$

$$B_{p+1} = c_{p+1} \frac{\bar{I} h_{p+1} i}{1 - i! h_{p+1} i} + B_p \frac{1}{1 - i! h_{p+1} i}; \quad (A 13)$$

(The initial conditions are still $A_0 = B_0 = 0$).

However, this improvement still does not solve the problem of relatively poor convergence of the algorithm, especially at low frequencies. The origin of the problem is hinted at by Eq. (A 2). Since we eliminated the T -segmentation used in the standard method, and now T is much longer (the whole simulation period), we are calculating $S_I(\omega)$ with a much smaller degree of spectral smoothing. The price for a better spectral resolution is the longer simulation time for the same accuracy. Therefore, to improve convergence, we have to re-introduce some time constant T_0 that would define the spectral smoothing $\omega \rightarrow \omega + i/T_0$. In principle, there are many ways to do this. For example, we can periodically (with period T_0) set to zero the value of B_p (in this case the algorithm becomes somewhat similar to the standard method). Alternatively, we can introduce a gradual cutoff of B_p , for example, multiplying the last term in Eq. (A 13) by $\exp(-h_{p+1} i/T_0)$, and so on.

We have used the following way of introducing T_0 , which is the best among those we had tried. For simplicity, let us consider first the algorithm without subtraction of \bar{I} , and average Eq. (A 6) over frequency (from $\omega = -1/h_1$ to $\omega = 1$) with the Lorentzian weight factor $(T_0 = \tau) = 1 + (\omega + i)^2 T_0^2$. The integral can be easily calculated using the residue theorem since all the poles of Eq. (A 6) are in the lower half of the complex plane; therefore, closing the integration contour in the upper half-plane, we will have only one pole at $\omega = i + i/T_0$. As a result, the only change in Eq. (A 6) after integration is that ω is replaced by $\omega + i/T_0$ (more correctly, by $i + i/T_0$, but for simplicity we change the notation from i back to ω). Therefore, the Lorentzian averaging over frequency in our algorithm exactly corresponds to replacing ω with $\omega + i/T_0$ in the iteration equations (A 9)–(A 10).

For the algorithm with \bar{I} subtraction, the Lorentzian averaging is a little more difficult, because of the extra poles in the equation for $h_{p+1} i$ at $\omega = i = h_k i$ (upper half-plane) and at $\omega = 0$. However, as seen from Eqs. (A 12)–(A 13), the pole at $\omega = 0$ is eventually canceled, while the poles at $\omega = i = h_k i$ remain only in the simple additive term in Eq. (A 12). Therefore, the recipe of replacing ω with $\omega + i/T_0$ still works for B_{p+1} , and the extra residue of the upper-half-plane pole should be simply added to

A_{p+1} . As a result, Eqs. (A 12){ (A 13) are replaced with

$$A_{p+1} = A_p + \frac{q_{p+1}^2}{1} + 2 \frac{q_{p+1} \bar{I} h_{p+1} i}{i (! + i=T_0) h_{p+1} i} B_p + \frac{2 \bar{I} h_{p+1} i q_{p+1} \bar{I} h_{p+1} i (1 + h_{p+1} i=T_0)}{1 + (! h_{p+1} i)^2 + 2 h_{p+1} i=T_0 + (h_{p+1} i=T_0)^2}; \quad (\text{A } 14)$$

$$B_{p+1} = q_{p+1} \frac{\bar{I} h_{p+1} i}{1 i (! + i=T_0) h_{p+1} i} + B_p \frac{1}{1 i (! + i=T_0) h_{p+1} i}; \quad (\text{A } 15)$$

while the rest of the algorithm does not change.

The introduction of Lorentzian smoothing greatly improves the convergence of the algorithm. However, it gives rise to another difficulty. The problem is that the averaging over frequency increases the \bar{I} -function contribution from $S_I(0)$ due to average current, and the trick of the standard method, discussed above, is impossible for Lorentzian averaging [in contrast to Eq. (A 2), in which the convolution function contains zeros]. Formally, our algorithm subtracts \bar{I} beforehand; however, in a real simulation \bar{I} is not known exactly (note that the estimated value of \bar{I} can be improved during the course of simulation). It can be shown that the inaccuracy $\Delta \bar{I}$ in the

average current estimate used in Eqs. (A 14){ (A 15) brings to $S_I(!)$ the extra contribution

$$S_I(!) = 4T_0 (!)^2 = 1 + !^2 T_0^2 : \quad (\text{A } 16)$$

This contribution can be subtracted from $S_I(!)$ at the end of the simulation run, when a better estimate of \bar{I} is known and the difference from the initially used estimate can be calculated. Actually, the value of \bar{I} used in Eqs. (A 14){ (A 15) can be periodically (sufficiently rare) updated during the simulation run; in this case $(!)^2$ in Eq. (A 16) can naturally be replaced with the time-weighted value.

With these modifications, the advanced algorithm becomes significantly faster and more convenient than the standard algorithm. A accurate comparison of their efficiencies is not straightforward because both methods have adjustable parameters. (T in the standard method and T_0 in the new method both affect the smoothing of the spectral density and the convergence speed; the choice of too short T could also lead to incorrect results.) Crudely, the speed-up factor (the ratio of CPU times for the same accuracy using the two methods) for our typical simulation runs is two to three orders of magnitude.

-
- ¹ N. F. Mott and J. H. Davies, *Electronic Properties of Non-Crystalline Materials*, 2nd Ed., (Oxford Univ. Press, Oxford, 1979); N. F. Mott, *Conduction in Non-Crystalline Materials*, 2nd Ed. (Clarendon Press, Oxford, 1993).
- ² B. I. Shklovskii and A. L. Efros, *Electronic Properties of Doped Semiconductors* (Springer, Berlin, 1984).
- ³ *Hopping Transport in Solids*, edited by A. L. Efros and M. Pollak (Elsevier, Amsterdam, 1991).
- ⁴ Ya. Blanter and M. Buttiker, *Phys. Repts.* 336, 2 (2000).
- ⁵ K. A. Matsuoka and K. K. Likharev, *Phys. Rev. B* 57, 15613 (1998).
- ⁶ A. N. Korotkov and K. K. Likharev, *Phys. Rev. B* 61, 15975 (2000).
- ⁷ V. A. Sverdlov, A. N. Korotkov, and K. K. Likharev, *Phys. Rev. B* 63, 081302(R) (2001).
- ⁸ Yu. V. Nazarov and J. J. R. Struben, *Phys. Rev. B* 53, 15466 (1996).
- ⁹ Y. Kinkhabwala and A. N. Korotkov, *Phys. Rev. B* 62, R7727 (2000).
- ¹⁰ Notice that in contrast with some prior works, we do not include the factor 2 in the exponent. This difference should be kept in mind at the level of result comparison.
- ¹¹ N. S. Bakhvalov, G. S. Kazachka, K. K. Likharev, and S. I. Serdyukova, *Sov. Phys. JETP* 68, 581 (1989).
- ¹² C. W. Asshuber, *Computational Single-Electronics* (Springer, Berlin, 2001), Ch. 3.
- ¹³ W. Brenig, G. H. Dohler, and H. Heyszenau, *Phil. Mag.* 27, 1093 (1973).
- ¹⁴ D. N. Tsiganov and A. L. Efros, *Phys. Rev. Lett.* 88, 176602 (2002).
- ¹⁵ For a discussion of this issue, see Sec. 4.2 of Ref. 2.
- ¹⁶ S. Marianer and B. I. Shklovskii, *Phys. Rev. B* 46, 13100 (1992).
- ¹⁷ B. I. Shklovskii, *Fiz. Tekh. Poluprovodn.* 6, 2335 (1972) [*Sov. Phys. Semicond.* 6, 1964 (1973)].
- ¹⁸ This result emphasizes again that the validity of the master equation approach is very limited, and for most transport characteristics this equation fails to give quantitatively correct results for any region in the $[E; T]$ space.
- ¹⁹ A. N. Korotkov, D. V. Averin, K. K. Likharev, and S. A. Vasenko, in *Single-Electron Tunneling and Mesoscopic Devices*, edited by H. Koch and H. Luebbig (Springer, Berlin, 1992), p. 45.
- ²⁰ A. N. Korotkov, *Phys. Rev. B* 49, 10381 (1994).
- ²¹ B. I. Shklovskii, *Solid State Commun.* 33, 273 (1980); Sh. M. Kogan and B. I. Shklovskii, *Sov. Phys. Semicond.* 15, 605 (1981).
- ²² B. I. Shklovskii, *Phys. Rev. B* 67, 045201 (2003).
- ²³ In the case of hopping, the noise intensity is not exactly proportional to dc current, because the noise suppression factor depends on the ratio $L=L_c$, where the characteristic length L_c is itself a function of applied electric field, and hence (implicitly) of dc current – see Figs. 7-8 and their discussion below.
- ²⁴ D. V. Averin and K. K. Likharev, in *Mesoscopic Phenomena in Solids*, edited by B. L. Altshuler, P. A. Lee, and R. A. Webb (Elsevier, Amsterdam, 1991), p. 173.
- ²⁵ D. Stauffer and A. Aharony, *Introduction to Percolation Theory*, Rev. 2nd Ed., (Taylor and Francis Inc, Philadelphia, 1994).
- ²⁶ S. P. Obukhov, *Physica A* 101, 145 (1980).
- ²⁷ J. W. Essam, K. DeBell, J. Adler, and F. M. Bhatti, *Phys.*

- Rev. B 33, 1982 (1986).
- ²⁸ V. V. Kuznetsov, E. E. Mendez, X. Zuo, G. Snider, and E. Croke, Phys. Rev. Lett. 85, 397 (2000).
- ²⁹ S. H. Roshko, S. S. Safonov, A. K. Savchenko, W. R. Tribe, and E. H. Lindell, Physica E 12, 861 (2002).
- ³⁰ B. Derrida, Phys. Reports 301, 65 (1998).
- ³¹ K. Likharev, Proc. IEEE 87, 606 (1999).
- ³² V. A. Sverdlov, D. M. Kaplan, A. N. Korotkov, and K. K. Likharev, Phys. Rev. B 64, 041302(R) (2001).
- ³³ M. Amman, K. Mullen, and E. Ben-Jacob, J. Appl. Phys. 65, 339 (1989).
- ³⁴ MOSES (Monte-Carlo Single-Electron Simulator), versions 1.11 (for DOS and UNIX) and 1.2 (for UNIX only) are available online at <http://hana.physics.sunysb.edu/set/software/index.html>.